https://doi.org/10.5194/egusphere-2025-1377
Preprint. Discussion started: 28 March 2025
© Author(s) 2025. CC BY 4.0 License.

Asymmetric response of European near-surface wind speed to CO_2 removal

Zhi-Bo Li[1], Chao Liu[2], Cesar Azorin-Molina[3], Soon-Il An[2,4], Yang Zhao[5,6], Yang Xu[7], Jongsoo Shin[8], Deliang Chen[9,1], Cheng Shen[1,*]

[1] Regional Climate Group, Department of Earth Sciences, University of Gothenburg, Gothenburg, Sweden
[2] Irreversible Climate Change Research Center, Yonsei University, Seoul, South Korea
[3] Centro de Investigaciones sobre Desertificación, Consejo Superior de Investigaciones Científicas (CIDE, CSIC-UV-Generalitat Valenciana), Climate, Atmosphere and Ocean Laboratory (Climatoc-Lab), Moncada, Valencia, Spain
[4] Department of Atmospheric Sciences, Yonsei University, Seoul, South Korea
[5] Frontiers Science Center for Deep Ocean Multispheres and Earth System-Key Laboratory of Physical Oceanography-Institute for Advanced Ocean Studies-Academy of the Future Ocean, Ocean University of China, Qingdao, China
[6] College of Oceanic and Atmospheric Sciences, Ocean University of China, Qingdao, China
[7] Department of Atmospheric Science, Yunnan University, Kunming, China
[8] Woods Hole Oceanographic Institution, Woods Hole, MA, USA
[9] Department of Earth System Sciences, Tsinghua University, Beijing, China

***Corresponding author**: Cheng Shen (cheng.shen@gu.se)

Key words:

CO_2 removal; AMOC; near-surface wind; European wind; Asymmetric response; Northern hemisphere

https://doi.org/10.5194/egusphere-2025-1377
Preprint. Discussion started: 28 March 2025
© Author(s) 2025. CC BY 4.0 License.

Abstract

Understanding the changes in near-surface wind speed (NSWS) is crucial for weather extremes and wind energy management. This study examines the response of NSWS to atmospheric carbon dioxide (CO_2) removal using large ensemble simulations and the Carbon Dioxide Removal Model Intercomparison Project models. Our results indicate that increasing CO_2 levels lead to an overall reduction in the Northern Hemisphere (NH) extratropical NSWS over land. Subsequent CO_2 reduction during the early ramp-down period rapidly restores NH NSWS. However, this recovery stalls and enters a declining trend during the late ramp-down period, mainly due to opposite negative NSWS trends in Europe. Notably, the rapid recovery of simultaneous Atlantic Meridional Overturning Circulation (AMOC) counteracts the recovery of North Atlantic air meridional temperature gradient and the westerly jet by global cooling, therefore prolonging NH mid-latitudes NSWS weakening. Our findings underscore the pivotal role of AMOC in modulating NSWS under varying CO_2 concentrations and provides insights for future climate adaptation.

1 Introduction

The phenomena of terrestrial near-surface wind speed (~10 m above the ground; NSWS) "stilling" and "reversal" have been recognized for over a decade, yet significant gaps remain in understanding these processes (Wu et al., 2018; Zeng et al., 2019). Future projections of NSWS have garnered significant attention partly due to their implications for wind energy development (Karnauskas et al., 2018; Zeng et al., 2019; Zhang and Li, 2020; Pryor et al., 2021; Shen et al., 2024). Several studies have investigated the spatiotemporal variations of

https://doi.org/10.5194/egusphere-2025-1377
Preprint. Discussion started: 28 March 2025
© Author(s) 2025. CC BY 4.0 License.

NSWS in response to atmospheric carbon dioxide (CO_2) forcing in the coming years until the end of this century based on climate models, revealing global and regional variations driven by polar amplification and altered land-sea thermal gradients (Bichet et al., 2012; Karnauskas et al., 2018; Shen et al., 2021; Zha et al., 2021; Deng et al., 2022). Future projections using these models, mostly from the Coupled Model Intercomparison Project Phases 5 and 6 (CMIP5 and CMIP6) (Taylor et al., 2012; O'Neill et al., 2016), suggest a robust reduction in NSWS across the mid-latitudes of the Northern Hemisphere (NH) land in the 21st century, while an increase across the Southern Hemisphere (Karnauskas et al., 2018; Zha et al., 2021; Deng et al., 2022; Shen et al., 2022). However, the ideal CO_2 experiments in CMIP5 and CMIP6 mainly consider an increased carbon emission scenario by the end of the 21st century, and the further potential CO_2 removal impact on NSWS has not been studied. Understanding this response is crucial in light of imperative decarbonization goals and the extensive deployment of wind power (Lei et al., 2023).

The irreversibility and asymmetry of various climate phenomena have been investigated under CO_2 ramp-up and ramp-down experiments using the global climate models. Many studies used “1pctCO_2” experiment as the ramp-up period, in which the CO_2 concentration gradually increases at a rate of 1% per year for 140 years until it quadruples (Eyring et al., 2016). On this basis, different scenarios of ramp-down period are performed to study the reversibility of CO_2 induced climate change (Wu et al., 2010; Cao et al., 2011; Boucher et al., 2012; MacDougall, 2013; Wu et al., 2014; Ma et al., 2016; Field and Mach, 2017; Ehlert and Zickfeld, 2018). Meanwhile, the Carbon Dioxide Removal Model Intercomparison Project (CDRMIP) in CMIP6 has been launched to provide 1pctCO_2-carbon dioxide removal

https://doi.org/10.5194/egusphere-2025-1377
Preprint. Discussion started: 28 March 2025
© Author(s) 2025. CC BY 4.0 License.

experiment as the ramp-down period, in which the climate initiates from the end of the 1pctCO_2 experiment and the evolution of CO_2 concentration mirrors that in the 1pctCO_2 experiment (Keller et al., 2018). And the projection uncertainties related to different model frameworks could also be investigated by these experiments (Zhang et al., 2023; Jin et al., 2024; Su et al., 2024).

Following the CDRMIP protocol (Keller et al., 2018), An et al. (2021) conducted large-ensemble simulations of CO_2 ramp-up and ramp-down simulations using the Community Earth System Model version 1.2 (CESM1.2). It is found that major ocean circulation systems, particularly the Atlantic Meridional Overturning Circulation (AMOC) shows a unique delayed recovery that significantly shapes the responses of other climatic factors (An et al., 2021; Oh et al., 2022). On this basis, following studies extend to the hydrological cycle (Yeh et al., 2021; Kim et al., 2022; Kug et al., 2022), El Niño–Southern Oscillation (Liu et al., 2023a, b; Pathirana et al., 2023), Hadley cell (Kim et al., 2023), gross primary productivity (Yang et al., 2024) and mid-latitude storm tracks (Hwang et al., 2024), all showing varying degrees of irreversibility. For the aspect of wind speed, Hwang et al. (2024) found that cyclone-related surface wind extremes become more frequent in southern North America and Europe in the late CO_2 removal period, while changes in the mean NSWS have received little attention.

Given that CESM has a reasonable performance in reproducing global historical NSWS (Shen et al., 2022), and the wind energy resources are expected to be significantly developed in the NH mid-latitudes (Pryor et al., 2020). We are motivated to investigate how NSWS in the NH mid-latitudes would respond to future CO_2 removal by using the CESM1.2 simulations and three available CMIP6 models participating the CDRMIP project.

https://doi.org/10.5194/egusphere-2025-1377
Preprint. Discussion started: 28 March 2025
© Author(s) 2025. CC BY 4.0 License.

2 Data and Method

2.1 CESM1.2 Simulations

The CESM1.2 (Hurrell et al., 2013) includes the atmosphere (Community Atmospheric Model version 5), ocean (Parallel Ocean Program version 2), sea ice (Community Ice Code version 4), and land models (Community Land Model version 4). The atmospheric model features a horizontal resolution of approximately 1° and 30 vertical levels (Neale et al., 2012). The ocean model comprises 60 vertical levels, with a longitudinal resolution of about 1° and a latitudinal resolution of about 0.3° near the equator, increasing gradually to about 0.5° near the poles (Smith et al., 2010). The land model includes the carbon-nitrogen cycle (Lawrence et al., 2011).

The experiment followed idealized CO_2 scenarios in two phases (An et al., 2021). In the first phase, the CO_2 concentration was held constant at 367 ppm, representing present-day levels, and the model is integrated for 900 years. In the second phase, the CO_2 concentration increased from 367 ppm to 1,478 ppm at a rate of 1% per year over 140 years (2001–2140: ramp-up period), then decreased back to 367 ppm at the same rate over the next 140 years (2141–2280: ramp-down period). After the ramp-down period, CO_2 levels were stabilized at 367 ppm for 220 years (2281–2500: stabilization period). This second phase was run with 28 ensemble members, each starting from different initial conditions taken from the present-day period, representing various phases of multi-decadal climate oscillations such as the Atlantic Multidecadal Oscillation and Pacific Decadal Oscillation. Such large ensemble simulations

https://doi.org/10.5194/egusphere-2025-1377
Preprint. Discussion started: 28 March 2025
© Author(s) 2025. CC BY 4.0 License.

provide a sufficient tool to separate the forced responses from internal variability, making it effective in assessing forced changes in regional NSWS (Li et al., 2019; Deser et al., 2020; Zha et al., 2021).

2.2 CDRMIP Simulations

We utilized CMIP6 models in the CDRMIP to verify the results of CESM1.2. Notably, CanESM5, MIROC-ES2L, and NorESM2-LM models are the only three available models with variables of "sfcWind" (near-surface wind speed) and "msftmz" (stream function, for calculating AMOC), and each model contains one realization. We compared terrestrial NSWS (60°S–70°N) climatology in their piControl experiments with the ERA5 (Hersbach et al., 2020), and found that the pattern correlation coefficients are 0.85, 0.81, 0.72, and 0.89 for CESM1.2, CanESM5, MIROC-ES2L, and NorESM2-LM, respectively. Indicating their reasonable ability in reproducing the large-scale characteristics of terrestrial NSWS.

2.3 AMOC Index

The AMOC index was calculated as the maximum stream function value at 26.7°N in the North Atlantic (0°N–70°N, 60°W–30°E), providing a robust measure of AMOC strength and variability across different simulation phases (An et al., 2021).

2.4 Statistical Methods

To facilitate consistent analysis, all data were bi-linearly interpolated to a uniform 1.5° × 1.5° grid for both latitude and longitude. All calculations related to NSWS are focused on the land regions. An 11-year running mean was used for all physical variables, unless otherwise stated. To clarify and quantify the contributions of global-mean surface air temperature and

https://doi.org/10.5194/egusphere-2025-1377
Preprint. Discussion started: 28 March 2025
© Author(s) 2025. CC BY 4.0 License.

AMOC to NSWS changes, we performed a bi-regression analysis. This analysis allowed us to assess the proportion of NSWS variance explained by each factor during different periods.

3 NSWS Responses to CO_2 Ramp-up and Ramp-down

In the CESM1.2 simulations, the annual global-mean surface air temperature (GMST) increases by about 5ºC from 2000 to 2140 (Figure 1a). This warming trend reverses during the ramp-down period (2141–2280) as CO_2 concentrations decrease, but the cooling trend is less pronounced than the prior warming. During the stabilization period (2281–2500), GMST remains approximately 1ºC above the year 2000 levels for about 40 years before gradually declining until 2500. Spatially, the ramp-up period shows pronounced warming over high-latitude land areas and less over the oceans (Figure S1a). The Subpolar North Atlantic (SNA) exhibits minimal warming, known as "warming hole" or "cold blob" (Chemke et al., 2020; Keil et al., 2020; Rahmstorf, 2024), and is likely due to reduced heat transport associated with a weakening AMOC under global warming (Zhang et al., 2019). Conversely, during the ramp-down period (2141–2280), most areas cool, including the SNA (Figure S1b). The asymmetric surface air temperature (SAT) trend over the SNA is mostly related to the late recovery of the AMOC during the late ramp-down period (2221–2280), which is influenced by increased salt advection feedback due to changes in the subtropic-to-subpolar salinity gradient and ocean stratification (An et al., 2021; Oh et al., 2022).

During the CO_2 ramp-up period (2001–2140), the NH-averaged (20°N–70°N) annual-mean NSWS decreased, consistent with projections by CMIP6 models (Zha et al., 2021; Shen

https://doi.org/10.5194/egusphere-2025-1377
Preprint. Discussion started: 28 March 2025
© Author(s) 2025. CC BY 4.0 License.

et al., 2022). The ramp-down period is divided into early (2141–2220) and late (2221–2280) ramp-down periods (An et al., 2021). During the early ramp-down period (2141–2220), NSWS in the NH extratropics quickly rebounds to 2000 levels at about double the rate of the ramp-up period. The corresponding SAT pattern features stronger cooling over the SNA (Figure S1c), similar to the ramp-up period, indicating a strengthened meridional SAT gradient. During the late ramp-down period (2221–2280), NSWS trend moderate across the NH extratropics (Figure 1b), accompanied by a notable warming trend over the SNA and weaker cooling trends over the high latitudes of the NH compared to the early ramp-down period (2141–2220) (Figures S1c–d). Throughout the stabilization period (2281–2500), NSWS trends in the NH continue to decline for several decades before gradually increasing towards the end of the period.

To investigate the regional reversibility of NSWS under CO_2 forcing, Figures 2a–d show the spatial patterns of NH NSWS trends during the ramp-up, ramp-down, early ramp-down, and late ramp-down periods, respectively. During the ramp-up period (2001–2140) (Figure 2a), significant negative NSWS trends dominate the mid-latitudes of the NH. During the ramp-down period (2141–2280), this spatial pattern reverses (Figure 2b), with a pattern correlation coefficient of -0.9 (P<0.01) between the ramp-up and ramp-down periods, highlighting a substantial impact of CO_2 on global NSWS patterns. Spatial discrepancies between two ramp-down periods are primarily observed over the Eurasia continent: during the early ramp-down period (2141–2220), NSWS shows marked positive trends (Figure 2c); however, these positive trends turn negative in Europe and diminish in North America and Central Asia in the late ramp-down period (2221–2280) (Figure 2d).

https://doi.org/10.5194/egusphere-2025-1377
Preprint. Discussion started: 28 March 2025
© Author(s) 2025. CC BY 4.0 License.

We further examined NSWS responses in three CMIP6 models from CDRMIP to testify the CESM1.2-based results (Figures S2 and S3). It is found that the time series of NSWS over the NH extratropics are generally similar across the three models (Figure S2), as are the spatial patterns of NSWS trends (Figure S3). However, there are also some evident inter-model differences between the CDRMIP models and the CESM1.2 model. A fast recovery of NSWS is observed in the NH extratropics in the CESM1.2 during the early ramp-down period (Figure 1b), while it shows symmetric changes in three CDRMIP models during the ramp-down period (Figure S2). The discrepancies are partly related to a different AMOC evolution in the CESM1.2, which will be discussed in the next section.

4 Effect of AMOC on Modulating the NH Extratropical NSWS

Previous studies suggested that hemispheric NSWS changes are influenced by the large-scale meridional SAT gradient (Zha et al., 2021; Deng et al., 2022; Shen et al., 2022; Li et al., 2024), with NH mid-latitude NSWS changes being closely linked to the westerly jet through the vertical downward transport of upper-level horizontal momentum (Shen et al., 2023; Shen et al., 2025). Moreover, the strength of the AMOC critically affects these regional patterns by modulating the meridional SAT gradient and the westerly jet through its control of the SNA temperature (Zhang et al., 2019; An et al., 2021; Hwang et al., 2024). Figure 3a shows the evolution of the AMOC index in the CESM1.2, revealing a weakening trend during the ramp-up period until 2200, followed by a rapid strengthening trend until 2300. Temporal changes of AMOC are similar among three CDRMIP models (Figure S4), with symmetric decreasing and increasing trends during ramp-up and ramp-down periods. The different responses of AMOC

https://doi.org/10.5194/egusphere-2025-1377
Preprint. Discussion started: 28 March 2025
© Author(s) 2025. CC BY 4.0 License.

would influence regional temperature gradient, further modulate regional atmospheric circulation (Hwang et al., 2024).

To disentangle the effects of CO_2 levels and AMOC on NSWS variations, we analyzed the temporal evolution of meridional SAT gradients and westerly jets across both the NH and North Atlantic (NA) (Figures 3b–e). The meridional SAT gradient was defined as the SAT difference between mid-latitude (60°N-90°N) and tropical (0°N-30°N) bands. Mid-latitude westerly jets were defined as the average 500 hPa zonal winds for 30°N–60°N. A significant negative correlation (-0.78, $P<0.01$) exists between the NH extratropical NSWS and the NH SAT gradient (Figure 3b), whereas a strong positive correlation (0.91, $P<0.01$) is detected with the NH westerly jet (Figure 3c). During the ramp-up period (2001–2140), the weakened NH SAT gradient contributed to a reduced westerly jet and a weakening NSWS trend across extratropics. The NH extratropical NSWS trend reverses in the early ramp-down period (2141–2220) as the NH SAT gradient and westerly jet recovers. However, in the late ramp-down period (2221–2280), the NH SAT gradient enhanced a bit (Figure 3b), while both the NH westerly jet (Figure 3c) and extratropical NSWS (Figure 1b) change slow, disregarding the CO_2-removal induced global cooling. These observations suggest an effect from the AMOC, which strongly modulates the SAT gradient in the NA, and thus local NSWS trends.

During the ramp-up period (2001–2140), the NA SAT gradient weaken by approximately 1°C (Figure 3d), a smaller change compared to the 6.5°C reduction in the NH SAT gradient (Figure 3b). Actually, the NA SAT gradient changes are modulated by two combined effects: CO_2-induced global warming/cooling and the AMOC strength (Zhang et al., 2019). This milder NA SAT gradient change is related to a weakened AMOC's role in transporting warm

https://doi.org/10.5194/egusphere-2025-1377
Preprint. Discussion started: 28 March 2025
© Author(s) 2025. CC BY 4.0 License.

water to the SNA, which partially offsets the hemisphere-scale SAT gradient weakening induced by global warming (Figure 3d). In the early ramp-down period (2141–2220), the synergistic effects of global cooling and a further weakened AMOC promote a stronger enhancement of the NA SAT gradient (Figure 3d) and westerly jet (Figure 3e). Conversely, during the late ramp-down period (2221–2280), the fast recovery of the AMOC dramatically increases warm water flow to the SNA (Figure S1d), diminishes the NA SAT gradient (Figure 3d) despite the prevailing global cooling effect from CO_2-removal, and leads to a weakened NA westerly jet (Figure 3e).

The annual-mean 500 hPa zonal wind patterns (Figure 4) reflect similar tendencies to those of NSWS in the NH, particularly across mid-latitudes where enhanced zonal winds correlate with increased NSWS (Figure 2), and vice versa. Throughout the ramp-up period (2001–2140), there is a general weakening trend of westerly jets over the mid-latitude regions of the Asian and North American continents, while regional westerlies intensify over NA and Europe (Figure 4a). The early ramp-down period (2141–2220) witnesses significant strengthening trend of NH westerly jets (Figure 4c), propelled by global cooling and a weakened AMOC (Figure S1c). During the late ramp-down period (2221–2280), recovery of the AMOC causes significant weakening of westerly jets over NA and Europe by reducing the NA SAT gradient (Zhang et al., 2019; An et al., 2021; Hwang et al., 2024) (Figures 3d–e, and S5d), which correspondingly weakens NSWS over Europe (Figure 2d).

To further demonstrate the effect of the AMOC on changes in the NA SAT gradient and westerly jet, Figure 5 displays the inter-ensemble correlation coefficients between the 28 ensemble members for the AMOC, NA SAT gradient, NA westerly jet, and European (30°N–

https://doi.org/10.5194/egusphere-2025-1377
Preprint. Discussion started: 28 March 2025
© Author(s) 2025. CC BY 4.0 License.

60°N, 5°W–60°E) NSWS. The cross-member correlations are not significant during the ramp-up period (2001–2140) but become prominent in the late ramp-down period (2221–2280), underscoring the crucial effect of AMOC recovery on weakening the NA SAT gradient and westerly jet, leading to strong reductions in European NSWS. These findings indicate that the fast recovery of the AMOC plays a dominant role in shaping the westerly jet during the late ramp-down period, and consequently, the extratropical NSWS.

Moreover, we performed bi-regression analysis using GMST and AMOC to fit the changes of NSWS in NH extratropics during three periods. During the ramp-up period (2001–2140), GMST and AMOC explain the variance of NH extratropical NSWS for 98% and 1.2%, respectively. During the early ramp-down period (2141–2220), GMST and AMOC explain 95.3% and 4.2% of the variance, respectively. While during the late ramp-down period (2221–2280), GMST and AMOC explain 24.5% and 73.2% of the variance, respectively. The regression results show changes in GMST make the dominant role in regulating NH extratropical NSWS during the ramp-up and early ramp-down periods, when AMOC shows gradually weakening trend. But the effect of AMOC plays a key role during the late ramp-down period due to the fast recovery of AMOC. The results are consistent with those in Fig. S6c, suggesting that the trends of the NSWS are not simply in phase with the evolution of either CO2 or the AMOC.

5 Summary and Outlook

In this study, we utilize a CESM1.2 CO_2 removal experiment to assess the response of NSWS to anthropogenic CO_2 emission levels. Our analyses reveal an asymmetric response of

https://doi.org/10.5194/egusphere-2025-1377
Preprint. Discussion started: 28 March 2025
© Author(s) 2025. CC BY 4.0 License.

the NH extratropical NSWS during the CO_2 ramp-up (2001–2140) and ramp-down (2141–2280) periods. Figure 6 summarizes the physical mechanisms about how CO_2 and AMOC heat transport modulate European NSWS changes. During the ramp-up period, NSWS shows decreasing trends in the NH extratropics. During the early ramp-down period, NSWS substantially intensifies, facilitated by the combined effects of a weakened AMOC and the global cooling induced by CO_2 removal. These conditions strengthened the meridional SAT gradient and the tropospheric westerly jet, enhancing NSWS at these latitudes. In contrast, during the late ramp-down period, a rapid recovery of the AMOC leads to significant reductions in the North Atlantic SAT gradient and westerly jet. This effect is stronger than the global cooling induced by CO_2 removal, markedly weakening NSWS over Europe and resulting in an NSWS decrease over the NH. The European NSWS changes follow anticlockwise trajectories in relation to CO_2 concentrations (Figure 7a), indicating stronger NSWS during the CO_2 removal period than during the CO_2 increasing period at identical CO_2 concentrations (Kim et al., 2022). Although there are also asymmetries of NSWS over Aisa and North America (Figures 7b–c), but the amplitudes are much weaker than that over Europe. These phenomena imply the effect of AMOC is crucial to European NSWS. Moreover, three models from the CDRMIP reasonably replicate NSWS changes over the extratropics. The reason why CDRMIP models can not reproduce the asymmetric NSWS response is due to the symmetric AMOC evolution during the ramp-down period, which means the AMOC's effects are linearly in these models.

Before this study, the impact of the AMOC on terrestrial NSWS changes had been less recognized. Our results advance the understanding in wind research community, offering

https://doi.org/10.5194/egusphere-2025-1377
Preprint. Discussion started: 28 March 2025
© Author(s) 2025. CC BY 4.0 License.

valuable insights into long-term NSWS dynamics. The enhanced NH NSWS during the early CO_2 removal period could significantly increase wind energy production (Pryor et al., 2020) but also heighten the risks of wind-related extremes (Hwang et al., 2024; Yu et al., 2024). Therefore, it is critical for monitoring efforts and climate policy formulations to consider these findings in their long-term climate strategies to optimize benefits and mitigate risks associated with wind energy and climate interventions.

Declaration of competing interests

The authors declare no conflicts of interest.

Acknowledgments

This work is supported by the Swedish Formas (2023-01648) and the Swedish Research Council (VR: 2021-02163). Z.-B. L. is also supported by the Swedish Formas (2020-00982). C.A-M. is also supported by the CSIC Interdisciplinary Thematic Platform (PTI) “PTI+ Clima y Servicios Climáticos” and the RED-CLIMA 2 (ref. LINCG24042). S.-I.A. is also supported by National Research Foundation of Korea grants funded by the Korean government (NRF-2018R1A5A1024958). C.S. is also supported by the Sven Lindqvists Forskningsstiftelse, Stiftelsen Längmanska kulturfonden (BA24-0484) and Adlerbertska Forskningsstiftelsen (AF2024-0069). The CESM simulation was conducted on the supercomputer supported by the National Center for Meteorological Supercomputer of Korea Meteorological Administration (KMA), the National Supercomputing Center with supercomputing resources, associated technical support (KSC-2021-CHA-0030), and the Korea Research Environment Open NETwork (KREONET).

https://doi.org/10.5194/egusphere-2025-1377
Preprint. Discussion started: 28 March 2025
© Author(s) 2025. CC BY 4.0 License.

Data Availability

All data used in this study are publicly available. The CESM1.2 outputs are available from https://data.mendeley.com/datasets/f5ry6hgxkw/2. CMIP6 outputs are available from the Earth System Grid Federation (https://esgf-data.dkrz.de/projects/esgf-dkrz/). And ERA5 reanalysis data are available from the European Centre for Medium-Range Weather Forecasts (https://cds.climate.copernicus.eu/cdsapp#!/dataset/reanalysis-era5-single-levels?tab=overview).

Supplementary Information

The manuscript contains supplementary materials.

References

An, S.-I., J. Shin, S.-W. Yeh, S.-W. Son, J.-S. Kug, S.-K. Min, and H.-J. Kim (2021). Global cooling hiatus driven by an AMOC overshoot in a carbon dioxide removal scenario, *Earth's Future, 9*, e2021EF002165. https://doi.org/10.1029/2021EF002165

Bichet, A., M. Wild, D. Folini, and C. Schar (2012). Causes for decadal variations of wind speed over land: Sensitivity studies with a global climate model, *Geophysical Research Letters*, *39*(11). https://doi.org/10.1029/2012GL051685

Boucher, O., P. R. Halloran, E. J. Burke, M. Doutriaux-Boucher, C. D. Jones, J. Lowe, M. A. Ringer, E. Robertson, and P. Wu (2012). Reversibility in an Earth System model in response to CO2 concentration changes, *Environmental Research Letters, 7*, 024013. https://doi.org/10.1088/1748-9326/7/2/024013

Cao, L., G. Bala, and K. Caldeira (2011). Why is there a short-term increase in global precipitation in response to diminished CO_2 forcing? *Geophysical Research Letters, 38*, L06703. https://doi.org/10.1029/2011GL046713

Chemke, R., L. Zanna, and L. M. Polvani (2020). Identifying a human signal in the North Atlantic warming hole. *Nature Communications, 11*(1), 1–7. https://doi.org/10.1038/s41467-020-15285-x

Deng, K., W. Liu, C. Azorin-Molina, S. Yang, H. Li, G. Zhang, L. Minola, and D. Chen (2022). Terrestrial stilling projected to continue in the Northern Hemisphere mid-latitudes, *Earth's Future, 10*(7), e2021EF002448. https://doi.org/10.1029/2021EF002448

Deser, C., F. Lehner, K. B. Rodgers, T. Ault, T. L. Delworth, P. N. DiNezio, A. Fiore, C. Frankignoul, J. C. Fyfe, and D. E. Horton (2020). Insights from Earth system model initial-condition large ensembles and future prospects, *Nature Climate Change*, *10*(4),

https://doi.org/10.5194/egusphere-2025-1377
Preprint. Discussion started: 28 March 2025
© Author(s) 2025. CC BY 4.0 License.

277–286. https://doi.org/10.1038/s41558-020-0731-2

Ehlert, D, and K. Zickfeld (2018). Irreversible ocean thermal expansion under carbon dioxide removal, *Earth System Dynamics, 9*(1), 197–210. https://doi.org/10.5194/esd-9-197-2018

Eyring, V., S. Bony, G. A. Meehl, C. A. Senior, B. Stevens, R. J. Stouffer, and K. E. Taylor (2016). Overview of the Coupled Model Intercomparison Project Phase 6 (CMIP6) experiment design and organization, *Geoscientific Model Development, 9*, 1937–1958. https://doi.org/10.5194/gmd-9-1937-2016

Field, C. B., and K. J. Mach (2017). Rightsizing carbon dioxide removal, *Science, 356*(6339), 706–707. https://doi.org/10.1126/science.aam9726

Hersbach, H., B. Bell, P. Berrisford, S. Hirahara, A. Horányi, J. Muñoz-Sabater, J. Nicolas, C. Peubey, et al. (2020). The ERA5 global reanalysis, *Quarterly Journal of the Royal Meteorological Society, 146*(730), 1999-2049. https://doi.org/10.1002/qj.3803

Hurrell, J. W., M. M. Holland, P. R. Gent, S. Ghan, J. E. Kay, and P. J. Kushner (2013). The community earth system model: A framework for collaborative research. *Bulletin of the American Meteorological Society, 94*(9), 1339–1360. https://doi.org/10.1175/BAMS-D-12-00121.1

Hwang, J., S.-W. Son, C. I. Garfinkel, T. Woollings, H. Yoon, S.-I. An, S.-W. Yeh, S.-K., Min, J.-S. Kug, and J. Shin (2024). Asymmetric hysteresis response of mid-latitude storm tracks to CO_2 removal, *Nature Climate Change, 14*, 496–503. https://doi.org/10.1038/s41558-024-01971-x

Jin, J., D. Ji, X. Dong, K. Fei, R. Guo, J. He, Y. Yu, et al. (2024). CAS-ESM2.0 dataset for the Carbon Dioxide Removal Model Intercomparison Project (CDRMIP), *Advances in Atmospheric Sciences, 41*, 989–1000. https://doi.org/10.1007/s00376-023-3089-3

Karnauskas, K. B., J. K. Lundquist, and L. Zhang (2018). Southward shift of the global wind energy resource under high carbon dioxide emissions, *Nature Geoscience*, *11*(1), 38–43. https://doi.org/10.1038/s41561-017-0029-9

Keil, P., T. Mauritsen, J. Jungclaus, C. Hedemann, D. Olonscheck, and R. Ghosh (2020). Multiple drivers of the North Atlantic warming hole. *Nature Climate Change, 10*(7), 667–671. https://doi.org/10.1038/s41558-020-0819-8

Keller, D. P., A. Lenton, V. Scott, N. E. Vaughan, N. Bauer, D. Ji, C. D. Jones, et al. (2018). The Carbon Dioxide Removal Model Intercomparison Project (CDRMIP): rationale and experimental protocol for CMIP6, *Geoscientific Model Development, 11*(3), 1133–1160. https://doi.org/10.5194/gmd-11-1133-2018

Kim, S.-K., J. Shin, S.-I. An, H.-J. Kim, N. Im, S. Xie, J.-S. Kug, and S.-W. Yeh (2022). Widespread irreversible changes in surface temperature and precipitation in response to CO_2 forcing, *Nature Climate Change, 12*, 834–840. https://doi.org/10.1038/s41558-022-01452-z

Kim, S.-Y., Y.-J. Choi, S.-W. Son, K. M. Grise, P. W. Staten, S.-I. An, S.-W. Yeh, J.-S. Kug, S.-K. Min, and J. Shin (2023). Hemispherically asymmetric Hadley cell response to CO_2 removal, *Science Advances, 9*(30), eadg1801. https://doi.org/10.1126/sciadv.adg1801

Kug, J.-S., J.-H. Oh, S.-I. An, S.-W. Yeh, S.-K. Min, S.-W. Son, J. Kam, Y.-G. Ham, and J.

https://doi.org/10.5194/egusphere-2025-1377
Preprint. Discussion started: 28 March 2025
© Author(s) 2025. CC BY 4.0 License.

Shin (2022). Hysteresis of the intertropical convergence zone to CO_2 forcing, *Nature Climate Change, 12*, 47–53. https://doi.org/10.1038/s41558-021-01211-6
Lawrence, D. M., K. W. Oleson, M. G. Flanner, P. E. Thornton, S. C. Swenson, P. J. Lawrence, et al. (2011). Parameterization improvement sand functional and structural advances in Version 4 of the community land model. *Journal of Advances in Modeling Earth Systems, 3*(3), 1–27. https://doi.org/10.1029/2011ms000045
Lei, Y., Z. Wang, D. Wang, X. Zhang, H. Che, X. Yue, C. Tian, J. Zhong, L. Guo, L. Li, H. Zhou, L. Liu, and Y. Xu (2023). Co-benefits of carbon neutrality in enhancing and stabilizing solar and wind energy, *Nature Climate Change, 13*, 693–700. https://doi.org/10.1038/s41558-023-01692-7
Li, Z.-B., Y. Sun, T. Li, T. Hu, and Y. Ding (2019). Future changes in East Asian summer monsoon circulation and precipitation under 1.5 to 5 °C of warming, *Earth's Future*, *7*(12), 1391–1406. https://doi.org/10.1029/2019EF001276
Li, Z.-B., Y. Xu, H.-S. Yuan, Y. Chang, and C. Shen (2024). AMO footprint of the recent near-surface wind speed change over China, *Environmental Research Letters*, 19, 114031. https://doi.org/10.1088/1748-9326/ad7ee4
Liu, C., S.-I. An, F. Jin, J. Shin, J.-S. Kug, W. Zhang, M. F. Stuecker, X. Yuan, A. Xue, X. Geng, and S.-K. Kim (2023a). Hysteresis of the El Niño–Southern Oscillation to CO_2 forcing, *Science Advances, 9*(31), eadh8442. https://doi.org/10.1126/sciadv.adh8442
Liu, C., S.-I. An, F. Jin, M. F. Stuecker, W. Zhang, J.-S. Kug, X. Yuan, J. Shin, A. Xue, X. Geng and S.-K. Kim (2023b). ENSO skewness hysteresis and associated changes in strong El Niño under a CO_2 removal scenario, *npj Climate and Atmospheric Science*, 6, 117. https://doi.org/10.1038/s41612-023-00448-6
Ma, J., G. R. Foltz, B. J. Soden, G. Huang, J. He, and C. Dong (2016). Will surface winds weaken in response to global warming? *Environmental Research Letters, 11*, 124012. https://doi.org/10.1088/1748-9326/11/12/124012
MacDougall. A. H., (2013). Reversing climate warming by artificial atmospheric carbon-dioxide removal: Can a Holocene-like climate be restored? *Geophysical Research Letters, 40*(20), 5480–5485. https://doi.org/10.1002/2013GL057467
Neale, R. B., C.-C. Chen, A. Gettelman, P. H. Lauritzen, S. Park, D. L. Williamson, et al. (2012). Description of the NCAR community atmosphere model (CAM 5.0). NCAR Tech. Note NCAR/TN-486+ STR (pp. 1–12). National Center for Atmospheric Research.
Oh, J.-H., S.-I. An, J. Shin, and J.-S. Kug (2022). Centennial memory of the Arctic Ocean for future Arctic climate recovery in response to a carbon dioxide removal. *Earth's Future, 10*(8), e2022EF002804. https://doi.org/10.1029/2022EF002804
O'Neill, B. C., C. Tebaldi, D. P. Van Vuuren, V. Eyring, P. Friedlingstein, G. Hurtt, R. Knutti, E. Kriegler, et al. (2016). The scenario model intercomparison project (ScenarioMIP) for CMIP6, *Geoscientific Model Development*, *9*(9), 3461–3482. https://doi.org/10.5194/gmd-9-3461-2016
Pathirana, G., J.-H. Oh, W. Cai, S.-I. An, S.-K. Min, S.-Y. Jo, J. Shin, and J.-S. Kug (2023). Increase in convective extreme El Niño events in a CO_2 removal scenario, *Science Advances, 9*(25), eadh2412. https://doi.org/10.1126/sciadv.adh2412
Pryor, S., and R. J. Barthelmie (2021). A global assessment of extreme wind speeds for wind

https://doi.org/10.5194/egusphere-2025-1377
Preprint. Discussion started: 28 March 2025
© Author(s) 2025. CC BY 4.0 License.

energy applications, *Nature Energy*, *6*(3), 268–276. https://doi.org/10.1038/s41560-020-00773-7

Pryor, S., R. J. Barthelmie, M. S. Bukovsky, L. R. Leung, and K. Sakaguchi (2020). Climate change impacts on wind power generation, *Nature Reviews Earth & Environment*, *1*(12), 627–643. https://doi.org/10.1038/s43017-020-0101-7

Rahmstorf, S (2024). Is the Atlantic overturing circulation approaching a tipping point? *Oceanography, 37*(3), 16–29. https://doi.org/10.5670/oceanog.2024.501

Shen, C., J. Zha, D. Zhao, J. Wu, W. Fan, M. Yang, and Z.-B. Li (2021). Estimating centennial-scale changes in global terrestrial near-surface wind speed based on CMIP6 GCMs, *Environmental Research Letters*, *16*(8), 084039. https://doi.org/10.1088/1748-9326/ac1378

Shen, C., J. Zha, Z.-B. Li, C. Azorin-Molina, K. Deng, L. Minola, and D. Chen (2022). Evaluation of global terrestrial near-surface wind speed simulated by CMIP6 models and their future projections, *Annals of the New York Academy of Sciences*, *1518*(1), 249–263. https://doi.org/10.1111/nyas.14910

Shen, C., H. Yuan, Z.-B. Li, X. Yang, L. Minola, Y. Chang, and D. Chen (2023). March near-surface wind speed hiatus over China since 2011, *Geophysical Research Letters*, *50*(15), e2023GL104230. https://doi.org/10.1029/2023GL104230

Shen, C., Z.-B. Li, H. Yuan, Y. Yu, Y. Lei, and D. Chen (2024). Increases of offshore wind potential in a warming world, *Geophysical Research Letters*, *50*(15), e2024GL109494. https://doi.org/10.1029/2024GL109494

Shen, C., Z.-B. Li, F. Liu, H. W. Chen, and D. Chen (2025). A robust reduction in near-surface wind speed after volcanic eruptions: Implications for wind energy generation, *The Innovation*, 6(1), 100734. https://doi.org/10.1016/j.xinn.2024.100734

Smith, R., P. Jones, B. Briegleb, F. Bryan, G. Danabasoglu, J. Dennis, et al. (2010). The parallel ocean program (POP) reference manual ocean component of the community climate system model (CCSM) and community earth system model (CESM). LAUR-01853 (pp. 1–140).

Su, X., G. Huang, L. Wang, and T. Wang (2024). Global drought changes and attribution under carbon neutrality scenario, *Climate Dynamics, 62*, 7851–7868. https://doi.org/10.1007/s00382-024-07310-2

Taylor, K. E., R. J. Stouffer, and G. A. Meehl (2012). An overview of CMIP5 and the experiment design, *Bulletin of the American Meteorological Society, 93*(4), 485–498. https://doi.org/10.1175/BAMS-D-11-00094.1

Wu, J., J. Zha, D. Zhao, and Q. Yang (2018). Changes in terrestrial near-surface wind speed and their possible causes: an overview, *Climate Dynamics*, *51*(5–6), 2039–2078. https://doi.org/10.1007/s00382-017-3997-y

Wu, P., J. Ridley, A. Pardaens, R. Levine, and J. Lowe (2014). The reversibility of CO_2 induced climate change, *Climate Dynamics, 45*, 745–754. https://doi.org/10.1007/s00382-014-2302-6

Wu, P., R. Wood, J. Ridley, and J. Lowe (2010). Temporary acceleration pf the hydrological cycle in response to a CO_2 rampdown, *Geophysical Research Letters, 37*(12), L043730. https://doi.org/10.1029/2010GL043730

© Author(s) 2025. CC BY 4.0 License.

Yang, Y.-M., J. Shin, S.-W. Park, J.-H. Park, S.-I. An, J.-S., Kug, S.-W. Yeh, et al. (2024). Fast reduction of Atlantic SST threatens Europe-wide gross primary productivity under positive and negative CO2 emissions. *npj Climate and Atmospheric Science, 7*(1), 117. https://doi.org/10.1038/s41612-024-00674-6

Yeh, S.-W., S.-Y. Song, R. P. Allan, S.-I. An, and J. Shin (2021). Contrasting response of hydrological cycle over land and ocean to a changing CO_2 pathway, *npj Climate and Atmospheric Science, 4*, 53. https://doi.org/10.1038/s41612-021-00206-6

Yu, Y., Z.-B. Li, Z. Yan, H. Yuan, and C. Shen (2024). Projected emergence seasons of year-maximum near-surface wind speed, *Geophysical Research Letters*, *51*(2). https://doi.org/10.1029/2023GL107543

Zeng, Z., A. D. Ziegler, T. Searchinger, L. Yang, A. Chen, K. Ju, S. Piao, L. Z. Li, P. Ciais, and D. Chen (2019). A reversal in global terrestrial stilling and its implications for wind energy production, *Nature Climate Change*, *9*(12), 979–985. https://doi.org/10.1038/s41558-019-0622-6

Zha, J., C. Shen, Z.-B. Li, J. Wu, D. Zhao, W. Fan, M. Sun, C. Azorin-Molina, and K. Deng (2021). Projected changes in global terrestrial near-surface wind speed in 1.5° C–4.0° C global warming levels, *Environmental Research Letters*, *16*(11), 114016. https://doi.org/10.1088/1748-9326/ac2fdd

Zha, J., C. Shen, J. Wu, D. Zhao, W. Fan, H. Jiang, and T. Zhao (2023). Evaluation and projection of changes in daily maximum wind speed over China based on CMIP6. *Journal of Climate, 36*(5), 1503–1520. https://doi.org/10.1175/JCLI-D-22-0193.1

Zhang, R., R. Sutton, G. Danabasoglu, Y. O. Kwon, R. Marsh, S. G. Yeager, D. E. Amrhein, and C. M. Little (2019). A review of the role of the Atlantic meridional overturning circulation in Atlantic multidecadal variability and associated climate impacts, *Reviews of Geophysics*, *57*(2), 316–375. https://doi.org/10.1029/2019RG000644

Zhang, S., and X. Li (2020). Future projections of offshore wind energy resources in China using CMIP6 simulations and a deep learning-based downscaling method, *Energy*, *217*, 119321. https://doi.org/10.1016/j.energy.2020.119321

Zhang, S., X. Qu, G. Huang, and P. Hu (2023). Asymmetric response of South Asian summer monsoon rainfall in a carbon dioxide removal scenario, *npj Climate and Atmospheric Science, 6*(1), 10. https://doi.org/10.1038/s41612-023-00338-x

https://doi.org/10.5194/egusphere-2025-1377
Preprint. Discussion started: 28 March 2025
© Author(s) 2025. CC BY 4.0 License.

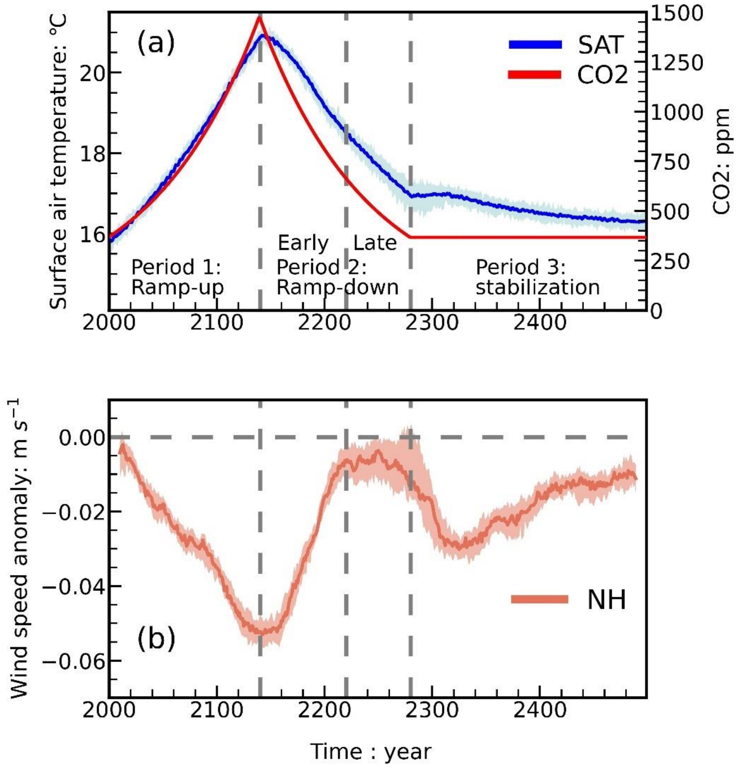

Figure 1. (a) Temporal changes of the annual global mean surface air temperature (SAT; unit: °C) (blue) and CO_2 concentration (unit: ppm) (red). The solid lines represent the ensemble means, while the shaded areas indicate the 25th to 75th percentile range across 28 members. Three dashed gray lines mark the years 2140, 2220, and 2280, highlighting important temporal milestones in the experiment. (b) Temporal changes of annual-mean terrestrial near-surface wind speed (NSWS; unit: m s^{-1}) over Northern Hemisphere (20°N–70°N) (orange). Anomalies are calculated relative to the average NSWS of the constant CO_2 scenario. An 11-year running mean has been applied to smooth out inter-annual variability.

https://doi.org/10.5194/egusphere-2025-1377
Preprint. Discussion started: 28 March 2025
© Author(s) 2025. CC BY 4.0 License.

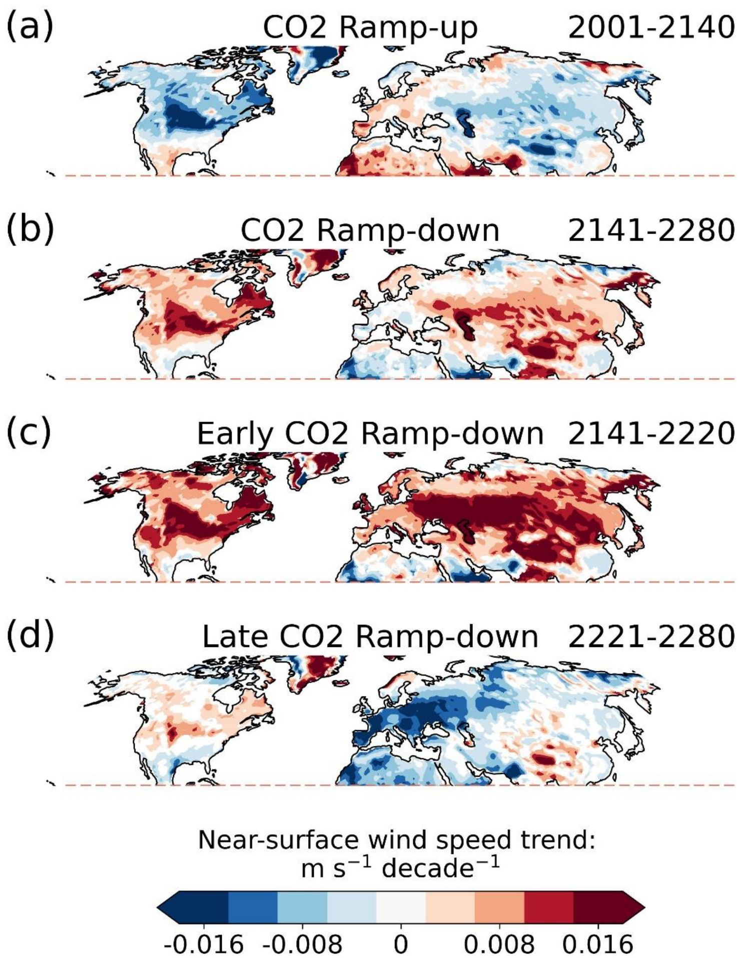

Figure 2. (a) Decadal trend in annual-mean near-surface wind speed (unit: m s^{-1} decade^{-1}) during the CO_2 ramp-up period (2001–2140). Grid points with shadings denote the tendencies are significant at the 0.05 level. (b–d) Same as (a), but for tendencies during the CO_2 ramp-down period (2141–2280), early CO_2 ramp-down period (2141–2220), and late CO_2 ramp-down period (2221–2280), respectively.

https://doi.org/10.5194/egusphere-2025-1377
Preprint. Discussion started: 28 March 2025
© Author(s) 2025. CC BY 4.0 License.

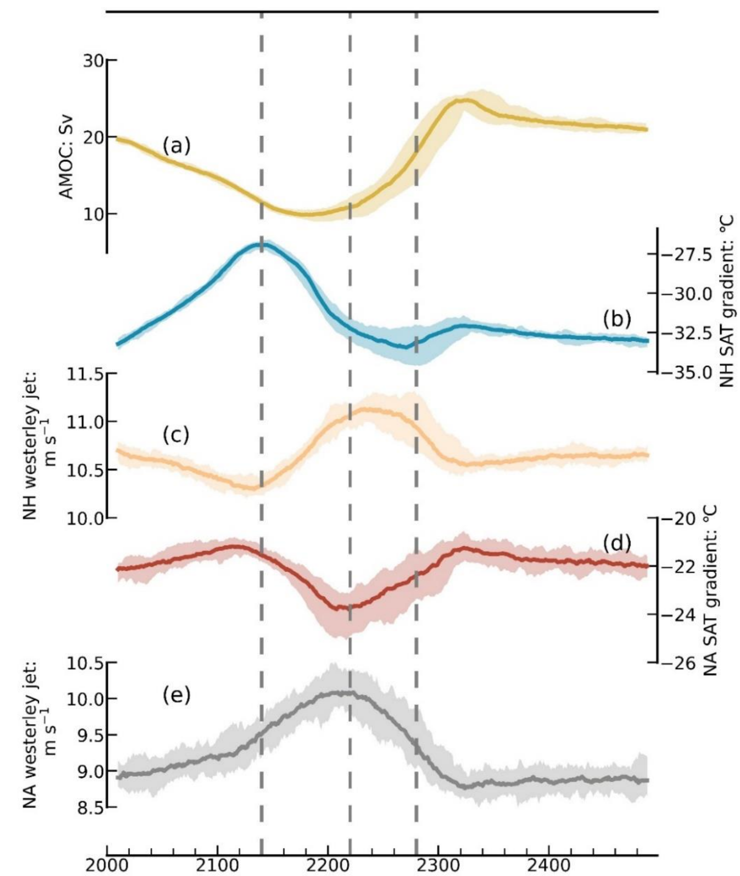

Figure 3. (a) Temporal changes of the Atlantic Meridional Overturning Circulation index (unit: Sv). The solid line represents the ensemble mean, and the shaded area shows the 25th to 75th percentile range of 28 ensemble members. Dashed gray lines at 2140, 2220, and 2280 denote significant temporal markers. (b–e) Same as (a), but for Northern Hemisphere (NH) surface air temperature gradient (60°N–90°N minus 0°N–30°N; in °C), NH westerly jet strength (the average for 30°N–60°N; in m s^{-1}) at 500 hPa, North Atlantic (NA, 60°W–30°E) surface air temperature gradient (60°N–90°N minus 0°N–30°N; in °C), and NA westerly jet strength (the average for 30°N–60°N, 60°W–30°E; in m s^{-1}) at 500 hPa, respectively. An 11-year running mean has been applied to smooth out inter-annual variability.

https://doi.org/10.5194/egusphere-2025-1377
Preprint. Discussion started: 28 March 2025
© Author(s) 2025. CC BY 4.0 License.

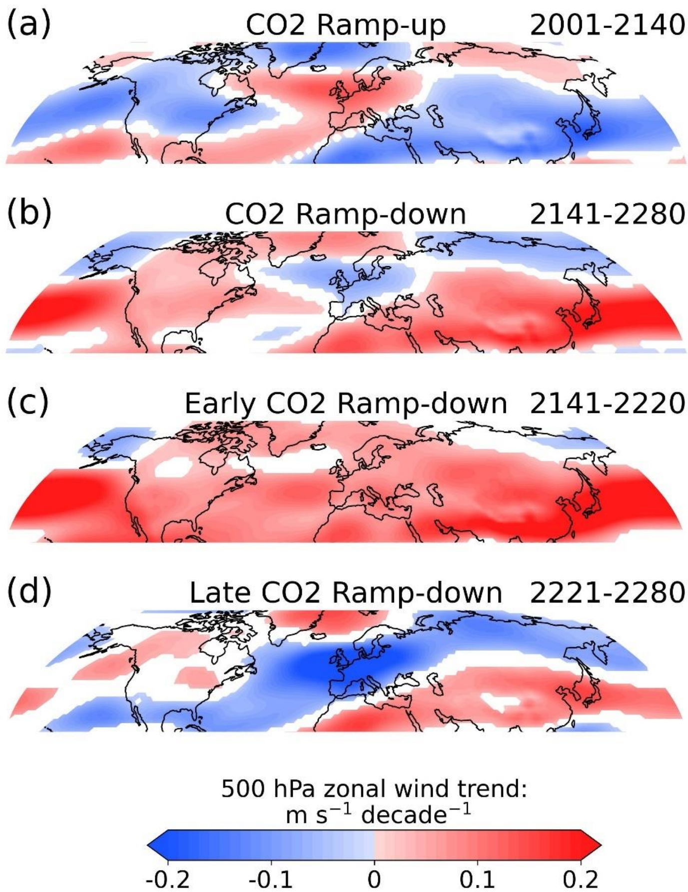

Figure 4. (a) Tendencies of ensemble-mean annual-mean 500 hPa zonal wind (unit: m s^{-1} decade^{-1}) during the CO_2 ramp-up period (2001–2140). Grid points with shadings denote the tendencies are significant at the 0.05 level. (b–d) Same as (a), but for tendencies during the CO_2 ramp-down period (2141–2280), early CO_2 ramp-down period (2141–2220), and late CO_2 ramp-down period (2221–2280), respectively.

https://doi.org/10.5194/egusphere-2025-1377
Preprint. Discussion started: 28 March 2025
© Author(s) 2025. CC BY 4.0 License.

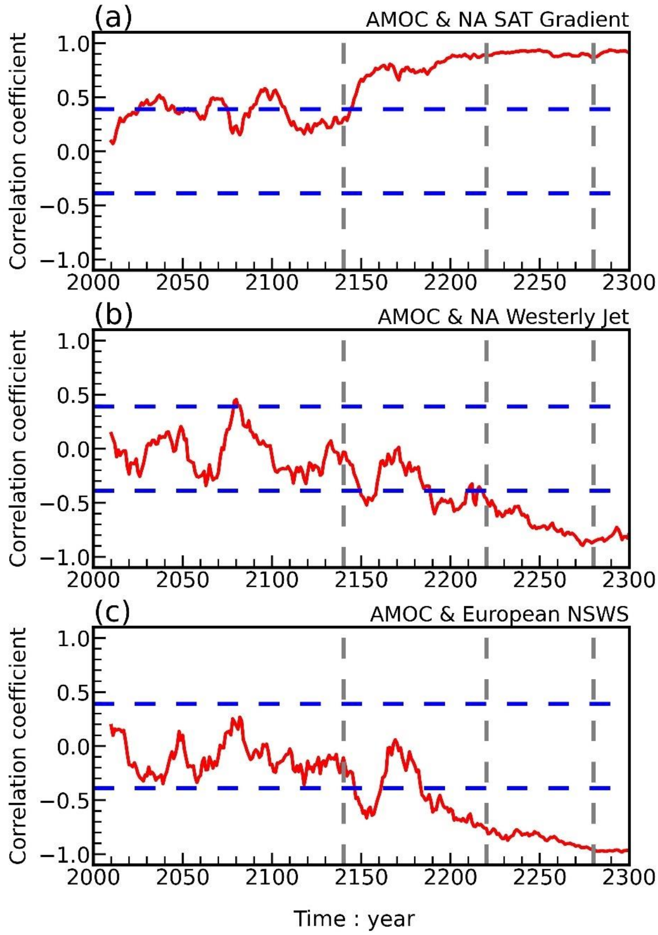

Figure 5. (a) Inter-ensemble correlation coefficients between the 28 ensemble members: the AMOC versus North Atlantic (NA, 60°W–30°E) surface air temperature (SAT) gradient (60°N–90°N minus 0°N–30°N) from 2000 to 2300. Three dashed gray lines denote 2140, 2220 and 2280, respectively. Two dashed blue lines denote the 0.05 significance level. (b) Same as (a), but for correlation coefficients between the AMOC and NA westerly jet strength (30°N–60°N, 60°W–30°E) at 500 hPa. (c) Same as (a), but for correlation coefficients between the AMOC and terrestrial near-surface wind speed (NSWS) over Europe (30°N–60°N, 5°W–60°E). An 11-year running mean has been applied to smooth out inter-annual variability.

https://doi.org/10.5194/egusphere-2025-1377
Preprint. Discussion started: 28 March 2025
© Author(s) 2025. CC BY 4.0 License.

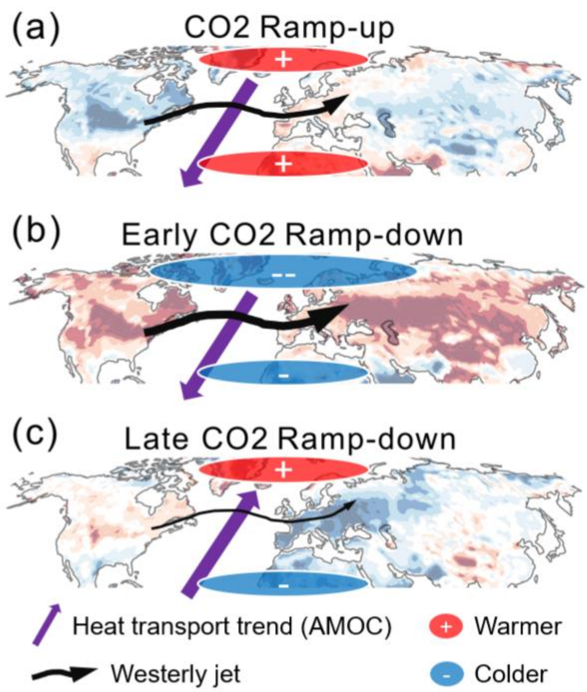

550

551 **Figure 6.** The physical mechanisms by which CO2 and Atlantic Meridional Overturning
552 Circulation modulate extratropical near-surface wind speed during three periods.

553

https://doi.org/10.5194/egusphere-2025-1377
Preprint. Discussion started: 28 March 2025
© Author(s) 2025. CC BY 4.0 License.

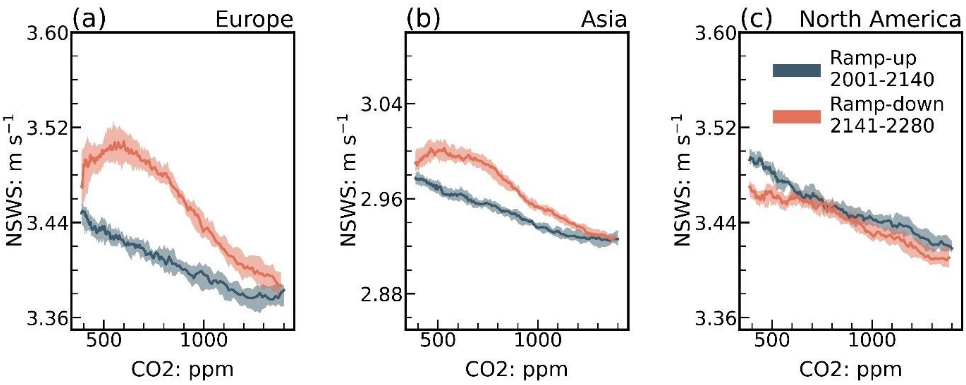

Figure 7. (a) Changes of terrestrial annual-mean near-surface wind speed over Europe (30°N–70°N, 5°W–50°E) as a function of CO_2 concentrations after 11-year running mean. The ramp-up (dark blue) and ramp-down (orange) are denoted with different colors. The solid line represents the ensemble mean, and the shaded area shows the 25th to 75th percentile range of 28 ensemble members. (b-c) Same as (a), but for Asia (20°N–70°N, 60°E–180°E) and North America (30°N–70°N, 170°W–50°W). The range of Y-axis is 0.25 m s^{-1} in each subplot.